AGU PUBLICATIONS

Tectonics

RESEARCH ARTICLE
10.1002/2015TC003824

Key Points:
- Dense material beneath the Tulare basin accounts for Pliocene subsidence
- Emplacement of a mantle load viscously thickened the lower crust beneath the basin.
- Removal of cold mantle lithosphere from the Sierra accounts for 1.5 km of uplift

Supporting Information:
- Text S1, Figures S1–S6, Table S1, and Caption of Data Set S1
- Data Set S1

Correspondence to:
W. Levandowski,
wlevandowski@usgs.gov

Citation:
Levandowski, W., and C. H. Jones (2015), Linking Sierra Nevada, California, uplift to subsidence of the Tulare basin using a seismically derived density model, *Tectonics*, *34*, doi:10.1002/2015TC003824.

Received 14 JAN 2015
Accepted 30 OCT 2015
Accepted article online 20 NOV 2015

Linking Sierra Nevada, California, uplift to subsidence of the Tulare basin using a seismically derived density model

Will Levandowski[1,2,3] and Craig H. Jones[1,2]

[1]Department of Geological Sciences, University of Colorado Boulder, Boulder, Colorado, USA, [2]CIRES, Boulder, Colorado, USA, [3]Now at U.S. Geological Survey, Colorado, USA

Abstract Seismic tomography has previously imaged the high-velocity "Isabella anomaly" southwest of the Sierra Nevada beneath the Tulare basin, a region of ~1 km of anomalous Pliocene subsidence. Additionally, it has been proposed that the eastern Sierra has risen 1–2 km since the Miocene in response to removal of dense lithospheric material. The Isabella anomaly has been variably interpreted as either this lithospheric material or a neutrally buoyant stalled fragment of the Farallon slab. To discriminate between these two, we estimate upper mantle density variations from seismic velocities and show that the estimated mass anomaly accords with 60 km of cold lithospheric material removed from beneath the southern Sierra, sufficient for 1.3 km of range uplift. A flexural model of the surface response to mantle loads predicts 1.3–1.7 km of anomalous subsidence of the Tulare basin, several hundred meters more than is observed. Nevertheless, beam-formed receiver functions show up to 10 km of crustal thickening beneath the basin, which we attribute to viscous response of the crust to mantle loading. This anomalous crustal thickness, the post-Miocene subsidence of the Tulare basin, and the uplift of the Sierra can all be explained by redistribution of cold continental mantle lithosphere; therefore, the Isabella anomaly is more plausibly such continental material than a stalled Farallon slab fragment.

1. Introduction

While the Great Valley of California has undergone late Miocene and more recent flexural subsidence due to asymmetric loading by the Sierra Nevada and Coast Ranges [*Rentschler and Bloch*, 1988], the Tulare subbasin in the southern San Joaquin Valley (Figure 1) hosts an additional 1.15 km of post-7 Ma sediment and 700 m of post-2.5 Ma sediment [*Saleeby et al*., 2013]. Further, the area east of the Tulare basin itself is anomalous in that Quaternary sediments aggrade up drainages into the western foothills of the Sierra Nevada; drainages elsewhere along the range front do not exhibit this pattern [*Saleeby and Foster*, 2004].

This area of anomalous subsidence (Figure 1) lies above a seismically fast body [*Raikes*, 1980] dubbed the Isabella anomaly that extends from near the base of the crust to ~250 km [*Jones et al*., 2014]. Because of a dearth of stations, signal-generated and anthropogenic noise, and weak crust-mantle impedance contrast, the Moho beneath the valley has been virtually unsampled by conventional receiver functions [*Zandt et al*., 2004; *Frassetto et al*., 2011].

This seismic structure stands in contrast to the range crest of the central and southern Sierra Nevada some 100 km to the east, where elevations locally exceeding 4 km overlie a well-imaged, 35–40 km deep Moho [*Frassetto et al*., 2011] and low-velocity upper mantle [*Jones et al*., 1994; *Fliedner et al*., 1996; *Ruppert et al*., 1998; *Fliedner and Klemperer*, 2000; *Jones et al*., 2014]. These low velocities coincide with high electrical conductivity [*Park*, 2004; *Ostos and Park*, 2012] consistent with warm asthenosphere to near Moho depths as also inferred from Pliocene-Quaternary mantle xenoliths [*Ducea and Saleeby*, 1996]. Heat flow values [*Saltus and Lachenbruch*, 1991] are too low to be in thermal equilibrium with asthenosphere near 40 km depth, requiring that any change in the upper mantle temperature must have occurred more recently than the 10 Ma timescale for heat diffusion across 40 km.

Between the range crest and the Tulare basin, the western foothills of the Sierra host westward thickening, high-velocity crust and high-velocity upper mantle [*Frassetto et al*., 2011; *Jones et al*., 2014]. Recent density estimates [*Levandowski et al*., 2013] suggest that the thermal structure of the upper mantle accounts for at

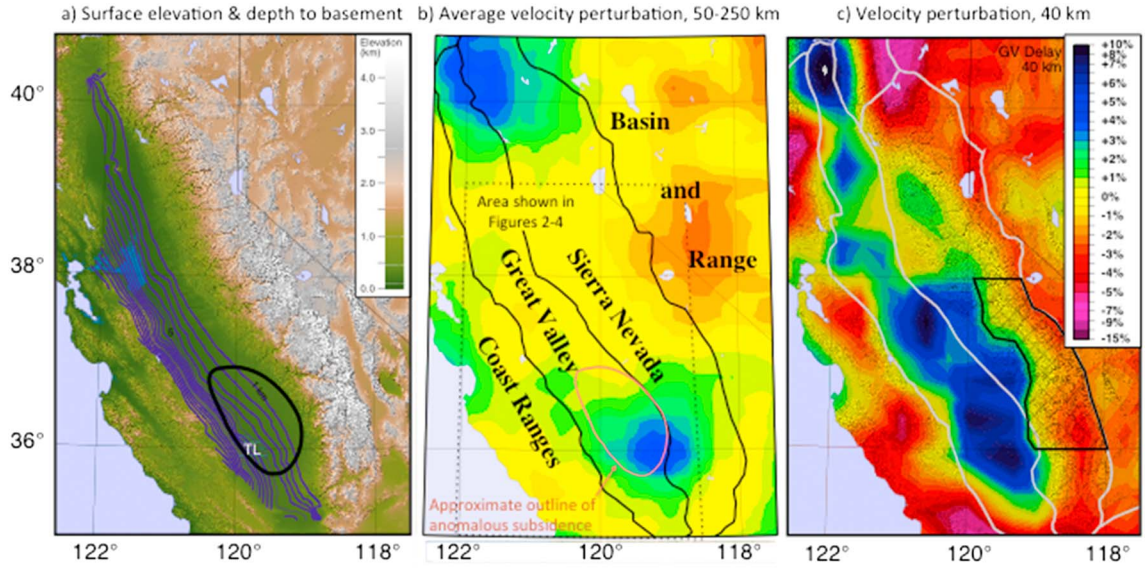

Figure 1. (a) Topography of the Sierra Nevada and surroundings; TL marks the position of historical Tulare Lake, the recent surface low point in the Tulare Basin. Contours of the depth of crystalline basement from *Wentworth et al.* [1995]; contour interval is 1 km. Heavy solid line represents the region of anomalous subsidence in the Tulare basin as drawn by *Saleeby et al.* [2013]. (b) Physiographic province boundaries overlain on the average *P* velocity perturbation of *Jones et al.* [2014] from 50 to 250 km. The high-velocity body near 119°W, 36°S is the Isabella anomaly. (c) Velocity at 40 km depth from *Jones et al.* [2014]. The inferred source region of the Isabella anomaly is the hachured polygon west of Owens Valley, east of the high-velocity lower crust, and between 36°N and 38°N: some 17,400 km^2.

least 1 km of relief between the range crest and the western foothills. Thus, if similar cold material had once existed under the range (e.g., hachured area in Figure 1c), its removal could readily account for 1 km of uplift.

The dichotomy in seismic character between the foothills and the range crest mirrors a temporal change in Sierran xenolith populations. A suite of ~10 Ma xenoliths records low-temperature pyroxenitic assemblages from depths currently below the Moho, but <3 Ma xenoliths were derived from warm peridotites at the same or shallower depths [*Ducea and Saleeby*, 1996, 1998; *Lee et al.*, 2000, 2001]. These observations and pressure-temperature (P-T) constraints from the xenoliths have been used to argue that some 60 km of cold, partially eclogitic lower crust and mantle lithosphere has been removed from beneath the southern Sierra since the Miocene.

Given its proximity to the Sierra and the fact that teleseismic *P* wave tomography [*Jones et al.*, 2014] images the Isabella anomaly as steeply plunging (>60° eastward) and extending just 100 km laterally but 200 km vertically, the Isabella anomaly may comprise this removed, sinking root, with its emplacement under the Tulare basin and southwestern foothills responsible for subsidence. Nevertheless, surface wave tomographic images of the same region [*Yang and Forsyth*, 2006; *Moschetti et al.*, 2010] generally show high-velocity material extending westward beneath the Coast Ranges, possibly to the Pacific-North America plate boundary, with a shallow (30°) eastward dip and a depth extent of only some 100 km. The latter evidence has been used to suggest that the Isabella anomaly is not dense continental lithosphere but a stalled fragment of the Monterey microplate, a Farallon remnant [*Benz and Zandt*, 1993; *Pikser et al.*, 2012; *Wang et al.*, 2013]. This oceanic lithosphere would have been young and thus relatively warm. Such a warm slab containing melt-depleted mantle could attain near-neutral buoyancy and cease subducting. *Pikser et al.* [2012] suggest that such water-poor mantle lithosphere would have a high enough viscosity to allow this material to couple to the Pacific plate and be transported under the North American plate almost 1000 km northward. In this case, the colocation of high-velocity material and the Tulare basin is purely coincidental, with subsidence instead caused by a combination of thrust loading by the Coast Ranges and a flexural moat associated with Sierran uplift.

Estimating the modern mantle density structure should discriminate between a neutrally buoyant slab and a cold lithospheric root. If Tulare basin subsidence and a substantial portion of Sierra Nevada uplift are cogenetic, resulting from redistribution of the mass presently in the Isabella anomaly, then two hypotheses remain

Table 1. Temperature and Pressure Dependence of Shear and Bulk Moduli and Thermal Expansivity

	Olivine: Fo92	Olivine: Fo90	Enstatite (OPX)	Diopside (CPX)	Garnet (Gt)	Spinel (Sp)
$G_{UnRelaxed}$, GPa	79.1	78.7	75.7	64.9	92.6	108.3
dG_{UR}/dT	−0.0138	−0.0136	−0.0119	−0.011	−0.0102	0.0094
dG_{UR}/dP	1.79	1.71	2.06	2	1.56	1.7
K_{UR}, GPa	129.4	129.5	107.8	114	171.2	196.7
dK_{UR}/dT	−0.0169	−0.018	−0.0268	−0.024	−0.0195	−0.0157
dK_{UR}/dP	5.13	4.56	9.6	4.6	4.93	5
α, 10^{-5}/°C	$-3.1–T_C/1350$ [*Bouhifd et al.*, 1996]	$-3.1–T_C/1350$ [*Bouhifd et al.*, 1996]	$-3.2–0.6\ T_c/1200$ [*Jackson et al.*, 2003]	−2.03 [*Hugh-Jones*, 1997]	$-2.31–5.96T_k\times10^{-4}–0.4358\ T_k^{-2}$ [*Afonso et al.*, 2005]	−2.94 [*Afonso et al.*, 2005]
$\Delta\rho$ per 1% Δv_p	12.37 kg/m^{-3} ± 0.09	11.87 kg/m^{-3} ± 0.08	8.31 kg/m^{-3} ± 0.05	4.08 kg/m^{-3} ± 0.04	12.02 kg/m^{-3} ± 0.16	12.82 kg/m^{-3} ± 0.17

to be tested: (1) that the modern *density* anomaly beneath the Tulare basin with respect to the rest of the Great Valley generates accommodation space for 700–1150 m of additional sediment and (2) that the integrated *mass* anomaly beneath the region of anomalous subsidence with respect to the upper mantle beneath the Sierra Nevada is of such a magnitude that its removal from beneath the Sierra would cause 1–2 km of range uplift. Previous models of the Tulare basin [*Saleeby and Foster*, 2004; *Le Pourhiet et al.*, 2006; *Saleeby et al.*, 2012] have chosen an a priori density. By contrast, we estimate density variations in the upper mantle from teleseismic *P* tomography, suggesting that if density estimates derived from wave speeds satisfy the two tests above, then the Isabella anomaly is likely cold, foundering lithosphere. If not, high wave speeds plausibly reflect melt-depleted, dry oceanic lithosphere with only a small thermal anomaly.

2. Mantle Density Calculation

Seismic velocity and density each depend on temperature and on composition. The two hypothesized origins of the Isabella anomaly—a dry, melt-depleted slab fragment and a cold, perhaps eclogitic portion of Sierran lithosphere—make different predictions about its density and more specifically how density relates to seismic velocity. Melt-depleted material is more buoyant than one would calculate by mapping velocity into temperature and then temperature into density variations, and eclogite is denser.

To quantify how well a purely thermal Isabella anomaly reproduces subsidence in the Tulare basin, we use mineral physics-based relationships among temperature, velocity, and density for olivine (Fo90 and Fo92), pyroxene (orthorhombic and monoclinic, and Fe and Mg end-members), garnet, and spinel. For each mineral

$$v_p(T,P) = \sqrt{\kappa(T,P) + \frac{4}{3}G(T,P) \Big/ \rho\,(T,P)} \tag{1}$$

The shear and bulk moduli (K and G) and density depend on temperature and pressure. Indeed, the thermal expansivity depends on temperature as well, such that a mineral with reference density ρ_0 at temperature T_0 has a density at a temperature T:

$$\rho(T) = \rho_0 \times \left(1 + \int_{T_0}^{T} \alpha(T)\mathrm{d}T\right) \tag{2}$$

We follow *Afonso et al.* [2005] in using laboratory data to calculate the derivative $\frac{\delta\rho/\delta T}{\delta v_P/\delta T}$. Table 1 provides the parameter values used to calculate unrelaxed moduli and the coefficient of thermal expansion. We then adjust the unrelaxed moduli for seismic frequency-, grain size-, and pressure-dependent anelastic effects [*Jackson and Faul*, 2010], using scripts provided by U. Faul (personal communication, 2015). For all six minerals examined, density is linearly related to *P* wave speed variations (quantified as percent difference from velocity at $T_0 = 1350$°C) with $r^2 > 0.999$ (Table 1).

Again, following Afonso et al., the bulk relationship between density and wave speed for fertile mantle (60% Fo90 + 16% OPX + 16% CPX + 8.0% Gt) at 0.2 Hz, 3 GPa, and 1 mm grain size is 10.0 ± 0.1 kg m^{-3}/1% Δv_p ± 0.1. The scaling for depleted mantle (60% Fo92 + 30% OPX + 5.0% CPX + 5.0% Gt) is similar: 10.7 ± 0.1 kg m^{-3}/1% Δv_p.

At 2 s period, these increase slightly, to 11.4 and 12.2 kg m^{-3}/1% Δv_p. Similarly, the values for 1 cm grains are 11.8 and 12.5 kg m^{-3}/1% Δv_p. Therefore, the range in plausible scaling of a velocity perturbation relative to an arbitrary reference to a density anomaly is 9.9 to 12.6 kg m^{-3}/1% Δv_p. Below, results will be presented for 11 kg m^{-3}/1% Δv_p with maximum and minimum estimates in parentheses.

In contrast to temperature, the compositional trends associated with melt depletion (increase in modal Mg and decrease in garnet and CPX) do not strongly affect *P* velocity but do lower density [*Schutt and Lesher*, 2010]. Using variation of Mg# as a proxy for melt depletion, a unit increase in Mg# correlates with a 17 kg m^{-3} density decrease and a negligible 0.07% v_p *increase*. Thus, a small amount of melt depletion could easily offset thermal antibuoyancy. Conversely, high levels of garnet and CPX (i.e., eclogite) increase to a much greater extent than *P* velocity. A 10% increase in weight percent of garnet and correlative increase in CPX is associated with only a 0.5% increase in v_p but a 36 kg/m^{-3} (1.1%) density increase [*Schutt and Lesher*, 2010]. Therefore, we will first assume that all upper mantle velocity variations are thermal in origin and calculate the attendant density variations. This density model will either underpredict, match, or overpredict the magnitude of post-Miocene subsidence, reflecting whether the Isabella anomaly is a stagnant, melt-depleted slab fragment, a sinking block of cold continental lithosphere, or foundering eclogitic lower crust/upper mantle material.

Teleseismic *P* wave tomographic models are superior to surface wave models for our application. Although *P* wave tomography tends to smear velocity anomalies vertically over the depth range of interest here, this smearing closely conserves the vertically integrated travel time [*Jones et al*., 2014] and thus the vertically integrated density anomaly. Therefore, the choice of which of the several models presented by Jones et al. to use is immaterial; they differ only because of the starting velocity model but invert the same set of delay times and therefore result in nearly identical vertically integrated travel times. By contrast, surface wave inversions tend to smear velocity anomalies laterally and would therefore not produce a robust estimate of vertically integrated density variations, which (convolved with the flexural filter of the lithosphere) create topographic relief.

We derive our density estimate from a *P* velocity model from *Jones et al*. [2014] that includes a set of station traveltime corrections for the deep sediments of the Great Valley ("GV delay" model). We include their 70 km, 120 km, 170 km, and 220 km layers, effectively considering the depth range from 55 to 245 km. Since we are primarily interested in lateral variations in density and mass, we remove the mean density from each layer (Figure 2). On average horizontally and vertically, the Isabella anomaly is 15 kg/m^{-3} denser (13–16.5 kg/m^{-3}) than regional upper mantle, with a maximum vertically averaged anomaly of 45 (41–52) kg m^{-3} and a peak anomaly of >100 kg/m^{-3} (Figure 2a), in the uppermost mantle beneath the foothills (though high-density upper mantle exists all along the western front of the Sierra, not just in the Isabella anomaly).

3. Flexural Model Parameterization

Our density estimates are discretized to the extent that the velocity model is reported as variations at a mesh of nodes. Thus, we solve for the surface deflection due to the load beneath each surface node and superpose these solutions.

As given by *Watts* [2001, equations (3.54) and (3.55)], the deflection $w(r)$ of a plate with flexural parameter β at radius r from the center of a cylindrical load of height h, radius R_d, and density anomaly $\Delta\rho$ is as follows:

$$w(r) = h\,\Delta\rho/\,(\rho_a - \rho_{\text{infill}})\,\left[\,R_d/\beta ker'(R_d/\beta)\,ber(r/\beta)\; - R_d/\beta kei'(R_d/\beta)\,bei(r/\beta) + 1\right] \tag{3a}$$

within the load (i.e., for $r < R_d$) and

$$w(r) = h\,\Delta\rho/\,(\rho_a - \rho_{\text{infill}})\,R_d/\beta\,\left[\,ber'(R_d/\beta)\,{*}ker(r/\beta)\; - bei'(R_d/\beta){*}kei(r/\beta)\right] \tag{3b}$$

outside of the load (i.e., $r >= R_d$).

Here ber, bei, ker, kei, ber′, bei′, ker′, and kei′ are zero-order Kelvin-Bessel functions and their derivatives. We assume values of 3300 kg/m^{-3} for asthenospheric density, ρ_a, and 1900 kg/m^{-3} for infill density (the upper kilometer or so of poorly indurated sediment). R_d is ~15 km, chosen so that the surface area of the cylinder top is equivalent to that of the tomography cells (25 × 28 km). The load density, $\Delta\rho$, is the average estimated density anomaly beneath the surface node from 55 to 245 km depth, and h is 190 km. Estimates of elastic thickness in the Sierra Nevada region range from 7 to 20 km [*Lowry et al*., 2000; *Kirby and Swain*, 2009;

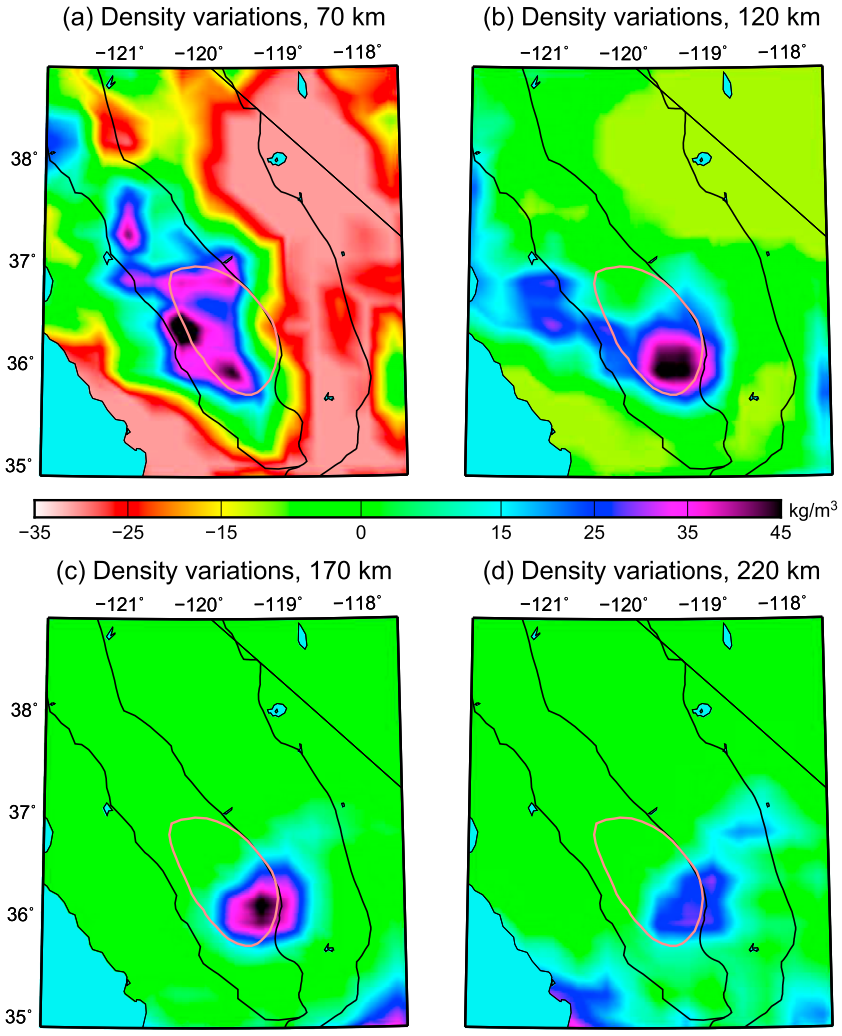

Figure 2. Density variations relative to the mean density in the Great Valley at the depths shown. *P* velocity variations at these depths [*Jones et al.*, 2014] are scaled to density variations as described in the text.

Lowry, 2012]. For simplicity, we discuss results for a uniform elastic thickness of ~15 km ($\beta = 40$ km) but have conducted trials with a range of β.

4. Flexural Model Results

The densities that we estimate from *P* wave tomography predict a regional maximum in subsidence in the Tulare basin (Figure 3) but overpredict its magnitude. If the modern mantle density structure is the result of post-Miocene mass redistribution, mantle loads should have allowed a maximum of 1.5 km (1.3–1.7 km) more sediment accumulation in the Tulare basin than in the rest of the Great Valley: 0.15–1.0 km greater than the observed 0.7–1.15 km.

A ~5 kg/m^{-3} decrease in the estimated density of the body would suffice to reproduce basin thickness patterns. Although melt depletion (commensurate with a 0.25 increase in Mg#) is a possible explanation for the mismatch between model and observation, the density anomaly of 11 kg/m^{-3} that best accords with post-Miocene subsidence is much closer to the 15 kg m^{-3} estimated here than to the negligible density anomaly of a stalled slab fragment.

As an alternative to our having overestimated the density of the Isabella anomaly, 30% of the load may be supported by any of several mechanisms. (If more than 30% of the load is attenuated, then observed

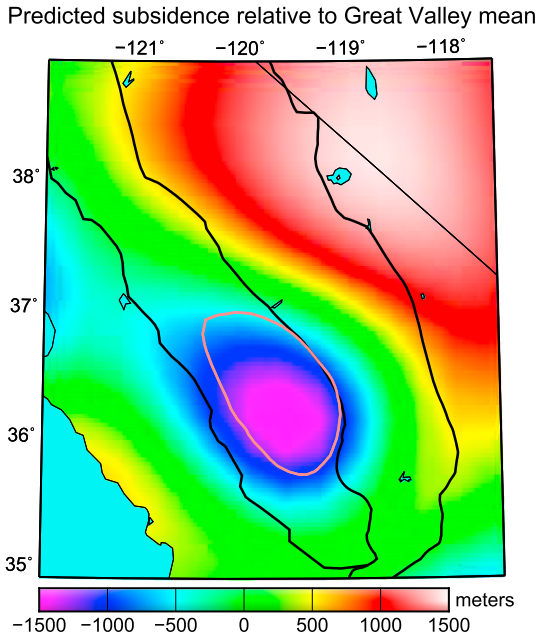

Figure 3. Flexurally modulated topography from loads between 50 and 250 km depth using 15 km elastic thickness. The Tulare basin is predicted to be a global maximum, with a maximum depth up to 1.5 km greater than the rest of the Great Valley. This model overestimates sedimentation by 0.35–0.8 km. Lower elastic thickness would produce more subsidence of the Tulare basin and stronger lithosphere less. With elastic thickness of 10 km, we predict up to 2.25 km of subsidence (1 km too much). With elastic thickness of 20 km, we predict 1.1 km of subsidence (the upper limit on anomalous sediment thickness).

subsidence requires a greater mass anomaly, permitting inclusion of eclogitic material but further negating neutral buoyancy of the Isabella anomaly.) First, in a viscous medium, the surface expression of a load decreases with increasing load depth [*Parsons and Daly*, 1983], but the Isabella anomaly appears contiguous to near the base of the crust, from which we infer a fairly efficient load transfer to the surface. Second, low-viscosity regions may not transmit vertical normal stress efficiently to the overlying surface. Despite its possible eastward plunge, however, the majority of the mass anomaly does not underlie material that is sufficiently slow that such decreased viscosity can be reasonably inferred (Figures 2a and 2b). Third, a body of radius R sinking through a viscous medium of viscosity μ at a velocity V is subject to Stokes' drag force.

$$S = 6\ \pi\ \mu RV \tag{4}$$

If the center of mass of the Isabella anomaly has descended from 70 to 130 km since 3–10 Ma, the range defined by xenoliths, its velocity is ~10 mm/yr. Using a radius of 50 km and an asthenospheric viscosity of 10^{19}–10^{20} Pa s [*Saleeby et al.*, 2012] (we will use $10^{19.5}$), this velocity would generate only 9×10^{15} N of drag, an order of magnitude less than the total load represented by the Isabella anomaly (calculated below). Finally, both conceptual [*Zandt et al.*, 2004] and numerical models [*Hoogenboom and Houseman*, 2006; *Molnar and Houseman*, 2013; *Stern et al.*, 2013] of lithospheric foundering have suggested that mantle loading may induce significant viscous thickening of the lower crust. If so, increased crustal buoyancy would partially counter the load of the Isabella anomaly, decreasing surficial subsidence; we explore such a possibility here.

5. Viscous Crustal Thickening

Based on earlier seismic studies and their own difficulty with identifying Moho on receiver functions (RFs), *Zandt et al.* [2004] proposed that the lowermost crust above the Isabella anomaly has thickened in response to post-Miocene mantle loading. In this conception, a geometrically complex Moho cusp produces low-amplitude Moho *P* to *S* mode conversions, explaining their absence from RFs presented in that paper. Near-surface scattering by the basin and complex structure in the ophiolitic foothills and a gradational or low-impedance contrast Moho could further obscure the Moho *Ps* signal [*Frassetto et al.*, 2011].

To resolve crustal thickness in the SW Sierran foothills, we have previously [*Levandowski*, 2007; *Levandowski et al.*, 2007; *Levandowski*, 2014] constructed "beam-formed" RFs [*Jones and Phinney*, 1998] on three-station subarrays (a full discussion is presented in the supporting information Text S1). Stations' radial and vertical traces for a given event are stacked, increasing signal-to-noise ratio by a factor √3 for arrivals common to all three stations and downweighting local signal-generated and other noise prior to deconvolution. Crustal thickness patterns from beamed RFs (Figure 4 and supporting information Text S1) are similar to single-station estimates [*Frassetto et al.*, 2011] where the two overlap: the lower elevation western foothills overlie thicker crust than the topographically highest southern Sierra. Additionally, these beamed RFs provide the first observed coherent Moho conversions from beneath the eastern Tulare basin and extend the trend of thickening crust into the basin, beneath diminishing topography and post-Miocene subsidence (Figure 4), where the crust is 5–10 km thicker than areas to the east northeast.

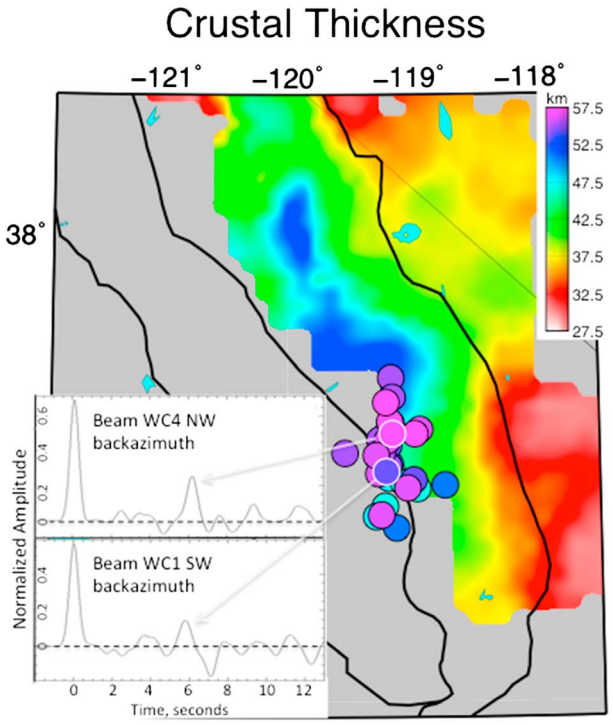

Figure 4. Crustal thickness map of the Sierra Nevada [after *Frassetto et al.*, 2011]. Additional constraints in the southwestern Sierra (circles) from beam-formed receiver functions [*Levandowski*, 2007] are shown as filled circles. The mean arrival on each subarray from each back azimuth quadrant is projected to the estimated conversion point using a crustal v_P/v_S of 1.72 (based on arrival times from local earthquakes in the western foothills of the central Sierra [*Hurd et al.*, 2006]) and a mean crustal v_P of 6.75 km/s [*Thurber et al.*, 2009]. Two example receiver functions from the southwestern foothills are shown. Note positive arrivals (Moho) near 6 s.

The lower crust beneath the eastern Tulare basin has a density, ρ_l, of 2950–3000 kg/m^{-3} [*Levandowski et al.*, 2013]. This additional 5–10 km, z_l, supports an additional elevation of

$$\Delta H = z_l(\rho_a - \rho_l)/\rho_a, \tag{5}$$

between 0.5 and 1 km. If crustal thickening is induced by a subcrustal load [*Hoogenboom and Houseman*, 2006; *Molnar and Houseman*, 2013], then we expect a corresponding 0.5–1 km reduction in downward deflection of the surface by the Isabella anomaly, thus removing the apparent discrepancy between the observed anomalous subsidence within the Tulare Basin and the subsidence predicted from the seismological model.

Inflow of crust above the Isabella anomaly is also consistent with seismically observed strain trajectories in this area. *Unruh et al.* [2014] noted a deflection in the principal strain rate axes in this region and showed that such a deflection was most consistent with an *upward* force above the Isabella anomaly. Such an upward force is inconsistent with the evolution of a sinking dense body in a uniform medium, but it is a likely outcome if crust has been entrained in the early stages of subsidence and then begins to relax as the sinker descends into the mantle [*Hoogenboom and Houseman*, 2006].

6. Linking the Isabella Anomaly to Sierra Nevada Uplift

The upper mantle density structure that is estimated from seismic wave speed alone nearly reproduces post-Miocene sedimentation patterns, leading us to reject the possibility that the Isabella anomaly comprises nearly neutrally buoyant oceanic slab material. We now investigate whether the Isabella anomaly may contain some 60 km of lowermost crust and mantle lithosphere removed from beneath the central and southern Sierra [*Biasi and Humphreys*, 1992; *Zandt*, 2003; *Jones et al.*, 2004]. On the east, the suggested source region (Figure 1c) is bounded by the extended Owens Valley—the western edge of the extended Basin and Range Province. Beneath the southwestern foothills of the Sierra, little mantle lithosphere could have existed during Farallon subduction just to the west, and high-velocity lower crust is intact; this high-velocity material thus marks the western boundary of the suggested source region. Along strike of the Sierra, the source region is roughly ~36–38°N; south of here, mantle lithosphere was likely removed during the Laramide orogeny [*Saleeby*, 2003], and removal of mantle lithosphere from the foothills and Central Valley to the north would produce uplift that is not observed. The surface area of this region is 17,400 km^2 (Figure 1c), and some 1–2 km of post-Miocene uplift thereof has been ascribed to this removal.

Both 2-D numerical models of convective instabilities [*Le Pourhiet et al.*, 2006; *Saleeby et al.*, 2012, 2013] and 3-D tomography [*Jones et al.*, 2014] suggest significant mixing of downwelling lithosphere and ambient asthenosphere. Nevertheless, mantle mixing and thermal equilibration with the surrounding asthenosphere preserve the integrated density anomaly over timescales of millions of years in the absence of vigorous convection, since

asthenosphere cools even as lithospheric material heats. In exploring Sierran uplift, the meaningful quantity is therefore the integrated mass of the Isabella anomaly compared to the mantle beneath the southern Sierra.

In the density model discussed above (Figure 2), the average density perturbation in the area between 120.5° and 118.5°W, between 35.5° and 37°N, and 55–245 km depth (5.6×10^6 km^3) with respect to the rest of the study region is 15.0 kg m^{-3}. The Isabella anomaly thus represents an excess mass of 8.4×10^{16} kg if it is a purely thermal perturbation. Following equations (3) and (5), removal of such mass from beneath the 17,400 km^2 region of the southern Sierra with asthenosphere would have raised the surface up to 1.3 km.

Because the total mass anomaly is rather insensitive to mantle mixing or heat diffusion over timescales of megayears, it can be used to estimate the original thickness of the material removed. Receiver function interpretations of *Frassetto et al.* [2011] and *Zandt et al.* [2004] and late Pleistocene, plagioclase-bearing xenoliths [*Ducea and Saleeby*, 1996] suggest that lithosphere was stripped to depths as shallow as the modern Moho (35–40 km). Based on surface heat flow and P-T constraints from Miocene xenoliths, *Molnar and Jones* [2004] estimate a Moho (35 km depth) temperature of 350°C at 10 Ma, consistent with refrigeration by the subducting Farallon slab. We assume that the lithosphere had an equilibrated, approximately linear geotherm of 10°C/km: $T(z) = 10z$. Relative to 1350°C, 3300 kg m^{-3} asthenosphere, the lithosphere had a density anomaly at 10 Ma, $\Delta T(z) = 1350°C – 10z$. The density anomaly as a function of depth, $\Delta\rho(z)$, is as in equation (2), and the mass anomaly per unit area is the integral of $\Delta\rho(z)$ from 35 km to the base of the material removed:

$$\int_{35\text{km}}^{\text{bottom}} \Delta\rho(z)\mathrm{d}z = \frac{\text{Mass}}{\text{Area}} = 8.4\times10^{16}\text{kg}/17,400\ \text{km}^2 \tag{6}$$

Solving for *bottom* gives a value of 95 km using α value for the fertile mantle composition discussed above and 87 km for depleted mantle.

Hence, we estimate that some 60 km of lithospheric material was removed. The deepest garnet pyroxenite xenoliths from the 10 Ma mantle lithosphere xenolith suite are from ~100 km depth [*Ducea and Saleeby*, 1996], consistent with the estimate of bottom we have derived from mass balance. The small amount of reequilibration of lithosphere with underlying asthenosphere between slab departure at 20 Ma and lithospheric removal at 3–10 Ma would only slightly increase the amount of lithosphere that must be removed.

7. Conclusions

Pliocene subsidence of the Tulare basin and 1.5 km of uplift of the Sierra Nevada may be cogenetic, resulting from redistribution of mass in the upper mantle. A seismically derived estimate of mantle density and flexural modeling show that mantle loads are capable of generating the observed 0.7–1.15 km of anomalous sediment accumulation in the Tulare basin and as much as 1 km more. Nevertheless, beamed receiver functions suggest an increase in crustal thickness of 10 km above the Isabella anomaly, coincident with deflections of the principal axes of the seismogenic strain rate field. We therefore suggest that the emplacement of a mantle load induced viscous thickening of the lower crust, attenuating surficial subsidence. The removal of the load now beneath the Tulare basin from beneath the southern Sierra would have resulted in 1.3 km of mean surface uplift of the range. Because such mass redistribution accounts for Tulare basin subsidence, crustal thickening, and post-Miocene Sierran uplift, we argue that it is unlikely that high wave speed material beneath the southeastern Central Valley is neutrally buoyant, likely precluding that it is dry, melt-depleted oceanic lithosphere. Instead, we favor the explanation that the Isabella anomaly comprises cold, dense lithospheric material stripped from beneath the Sierra Nevada.

Acknowledgments
Funded by NSF grant EAR-0607831, the *P* wave tomography was supported by NSF grant EAR-0454535. The beamed receiver functions were analyzed during an IRIS internship (W.B.L., University of Colorado, 2006; funded by NSF grant EAR-0453427 to Michael Hubenthal) and as undergraduate thesis partially supported by Princeton University research grants to W.B.L. The advice and guidance of Guust Nolet and Bob Phinney in the latter remain greatly appreciated. We are grateful for thorough and helpful reviews from Derek Schutt, Greg Houseman, Jason Saleeby, and Associate Editor Hersh Gilbert and to Ulrich Faul for his help in accounting for anelasticity. The mantle density model and the codes used for calculating the effects of temperature on seismic velocity and density and for flexural modeling are included in the supporting information.

References

Afonso, J. C., G. Ranalli, and M. Fernàndez (2005), Thermal expansivity and elastic properties of the lithospheric mantle: Results from mineral physics of composites, *Phys. Earth Planet. Inter.*, *149*(3–4), 279–306, doi:10.1016/j.pepi.2004.10.003.

Benz, H. M., and G. Zandt (1993), Teleseismic tomography: Lithospheric structure of the San Andreas fault system in northern and central California, in *Seismic Tomography: Theory and Practice*, edited by H. M. Iyer and K. Hirahara, pp. 440–465, Chapman and Hall, New York.

Biasi, G. P., and E. D. Humphreys (1992), *P*-wave image of the upper mantle structure of central California and southern Nevada, *Geophys. Res. Lett.*, *19*(11), 1161–1164, doi:10.1029/92GL00439.

Bouhifd, M. A., D. Andrault, G. Fiquet, and P. Richet (1996), Thermal expansion of forsterite up to the melting point, *Geophys. Res. Lett.*, *23*(10), 1143–1146, doi:10.1029/96GL01118.

Ducea, M., and J. Saleeby (1998), A case for delamination of the deep batholithic crust beneath the Sierra Nevada, California, *Int. Geol. Rev.*, *40*(1), 78–93, doi:10.1080/00206819809465199.

Ducea, M. N., and J. B. Saleeby (1996), Buoyancy sources for a large, unrooted mountain range, the Sierra Nevada, California: Evidence from xenolith thermobarometry, *J. Geophys. Res.*, *101*(B4), 8229–8244, doi:10.1029/95JB03452.
Fliedner, M. M., and S. L. Klemperer (2000), Three-dimensional seismic model of the Sierra Nevada arc, California, and its implications for crustal and upper mantle composition, *J. Geophys. Res.*, *105*(B5), 10,899–10,922, doi:10.1029/2000JB900029.
Fliedner, M. M., S. Ruppert, and S. W. Group (1996), Three-dimensional crustal structure of the southern Sierra Nevada from seismic fan profiles and gravity modeling, *Geology*, *24*(4), 367–370.
Frassetto, A. M., G. Zandt, H. Gilbert, T. J. Owens, and C. H. Jones (2011), Structure of the Sierra Nevada from receiver functions and implications for lithospheric foundering, *Geosphere*, *7*(4), 898–921, doi:10.1130/GES00570.1.
Hoogenboom, T., and G. A. Houseman (2006), Rayleigh-Taylor instability as a mechanism for corona formation on Venus, *Icarus*, *180*(2), 292–307, doi:10.1016/j.icarus.2005.11.001.
Hugh-Jones, D. (1997), Thermal expansion of $MgSiO_3$ and $FeSiO_3$ ortho- and clinopyroxenes, *Am. Mineral.*, *82*, 682–696.
Hurd, O., A. Frassetto, G. Zandt, H. Gilbert, and T. J. Owens (2006), Deep crustal earthquakes and repeating earthquakes in the west-central Sierra Nevada, western USA, *Eos Trans. AGU, 87(52)*, Fall Meet. Suppl., Abstract S43A-1360.
Jackson, I., and U. H. Faul (2010), Grainsize-sensitive viscoelastic relaxation in olivine: Towards a robust laboratory-based model for seismological application, *Phys. Earth Planet. Inter.*, *183*(1–2), 151–163, doi:10.1016/j.pepi.2010.09.005.
Jackson, J. M., J. W. Palko, D. Andrault, S. V. Sinogeikin, D. L. Lakshtanov, J. Wang, J. D. Bass, and C.-S. Zha (2003), Thermal expansion of natural orthoenstatite to 1473 K, *Eur. J. Mineral.*, *15*(3), 469–473, doi:10.1127/0935-1221/2003/0015-0469.
Jones, C. H., and R. A. Phinney (1998), Seismic structure of the lithosphere from teleseismic converted arrivals observed at small arrays in the southern Sierra Nevada and vicinity, California, *J. Geophys. Res.*, *103*(B5), 10,065–10,090, doi:10.1029/97JB03540.
Jones, C. H., H. Kanamori, and S. W. Roecker (1994), Missing roots and mantle "drips": Regional P_n and teleseismic arrival times in the southern Sierra Nevada and vicinity, California, *J. Geophys. Res.*, *99*(B3), 4567–4601, doi:10.1029/93JB01232.
Jones, C. H., G. L. Farmer, and J. Unruh (2004), Tectonics of Pliocene removal of lithosphere of the Sierra Nevada, California, *Geol. Soc. Am. Bull.*, *116*(11–12), 1408–1422, doi:10.1130/B25397.1.
Jones, C. H., H. Reeg, G. Zandt, H. Gilbert, T. J. Owens, and J. Stachnik (2014), *P*-wave tomography of potential convective downwellings and their source regions, Sierra Nevada, California, *Geosphere*, *10*(3), 505–533, doi:10.1130/GES00961.1.
Kirby, J. F., and C. J. Swain (2009), A reassessment of spectral Te estimation in continental interiors: The case of North America, *J. Geophys. Res.*, *114*, B08401, doi:10.1029/2009JB006356.
Le Pourhiet, L., M. Gurnis, and J. Saleeby (2006), Mantle instability beneath the Sierra Nevada Mountains in California and Death Valley extension, *Earth Planet. Sci. Lett.*, *251*(1–2), 104–119, doi:10.1016/j.epsl.2006.08.028.
Lee, C. T., Q. Yin, R. L. Rudnick, J. T. Chesley, and S. B. Jacobsen (2000), Osmium isotopic evidence for Mesozoic removal of lithospheric mantle beneath the Sierra Nevada, California, *Science*, *289*(5486), 1912–1916, doi:10.1126/science.289.5486.1912.
Lee, C. T., R. L. Rudnick, and G. H. Brimhall (2001), Deep lithospheric dynamics beneath the Sierra Nevada during the Mesozoic and Cenozoic as inferred from xenolith petrology, *Geochem. Geophys. Geosyst.*, *2*(12), doi:10.1029/2001GC000152.
Levandowski, W. B. (2007), Beam-formed receiver function analysis of the southern Sierra Nevada, California [A.B. Undergraduate]: Princeton Univ.
Levandowski, W. B. (2014), Geophysical investigations of the origins and effects of density variations in the crust and upper mantle beneath the western and central United States, PhD, Univ. of Colorado at Boulder, Boulder, Colo. [Available at http://gradworks.umi.com/36/21/3621364.html.]
Levandowski, W. B., C. H. Jones, G. Nolet, and R. A. Phinney (2007), Mysterious Moho beneath the southern Sierra Nevada, analyzed with beam-formed receiver functions AGU Fall Meeting, Abstract T33A-1148.
Levandowski, W., C. H. Jones, H. Reeg, A. Frassetto, H. Gilbert, G. Zandt, and T. J. Owens (2013), Seismological estimates of means of isostatic support of the Sierra Nevada, *Geosphere*, *9*(6), 1552–1561, doi:10.1130/GES00905.1.
Lowry, A. R. (2012), Estimates of elastic thickness (Te); surface heat flow data. [Available at http://aconcagua.geol.usu.edu/~arlowry/Data/WUS2000/README.html. (Accessed 2012).]
Lowry, A. R., N. M. Ribe, and R. B. Smith (2000), Dynamic elevation of the Cordillera, western United States, *J. Geophys. Res.*, *105*(B10), 23,371–23,390, doi:10.1029/2000JB900182.
Molnar, P., and G. A. Houseman (2013), Rayleigh-Taylor instability, lithospheric dynamics, surface topography at convergent mountain belts, and gravity anomalies, *J. Geophys. Res. Solid Earth*, *118*, 2544–2557, doi:10.1002/jgrb.50203.
Molnar, P., and C. H. Jones (2004), A test of laboratory based rheological parameters of olivine from an analysis of late Cenozoic convective removal of mantle lithosphere beneath the Sierra Nevada, California, USA, *Geophys. J. Int.*, *156*(3), 555–564, doi:10.1111/j.1365-246X.2004.02138.x.
Moschetti, M. P., M. H. Ritzwoller, F. C. Lin, and Y. Yang (2010), Crustal shear wave velocity structure of the western United States inferred from ambient seismic noise and earthquake data, *J. Geophys. Res.*, *115*, B10306, doi:10.1029/2010JB007448.
Ostos, L., and S. K. Park (2012), Foundering lithosphere imaged with magnetotelluric data beneath Yosemite National Park, California, *Geosphere*, *8*(1), 98–104, doi:10.1130/GES00657.1.
Park, S. K. (2004), Mantle heterogeneity beneath eastern California from magnetotelluric measurements, *J. Geophys. Res.*, *109*, B09406, doi:10.1029/2003JB002948.
Parsons, B., and S. Daly (1983), The relationship between surface topography, gravity anomalies, and temperature structure of convection, *J. Geophys. Res.*, *88*(B2), 1129–1144, doi:10.1029/JB088iB02p01129.
Pikser, J. E., D. W. Forsyth, and G. Hirth (2012), Along-strike translation of a fossil slab, *Earth Planet. Sci. Lett.*, *331–332*(C), 315–321, doi:10.1016/j.epsl.2012.03.027.
Raikes, S. A. (1980), Regional variations in upper mantle structure beneath southern California, *Geophys. J. Int.*, *63*(1), 1–22, doi:10.1111/j.1365-246X1980.tb02616.x.
Rentschler, M. S., and R. B. Bloch (1988), Flexural subsidence modeling of the Tertiary San Joaquin basin, California, in *Studies of the Geology of the San Joaquin Basin*, *Pac. Sect.*, vol. 60, pp. 29–52, Soc. of Econ. Paleontol. and Mineral., Los Angeles, Calif.
Ruppert, S., M. M. Fliedner, and G. Zandt (1998), Thin crust and active upper mantle beneath the southern Sierra Nevada in the western United States, *Tectonophysics*, *286*(1–4), 237–252.
Saleeby, J. (2003), Segmentation of the Laramide Slab—Evidence from the southern Sierra Nevada region, *Geol. Soc. Am. Bull.*, *115*(6), 655–668, doi:10.1130/0016-7606(2003)115<0655:SOTLSF>2.0.CO;2.
Saleeby, J., and Z. Foster (2004), Topographic response to mantle lithosphere removal in the southern Sierra Nevada region, California, *Geology*, *32*(3), 245–248, doi:10.1130/G19958.1.
Saleeby, J., L. Le Pourhiet, Z. Saleeby, and M. Gurnis (2012), Epeirogenic transients related to mantle lithosphere removal in the southern Sierra Nevada region, California, part I: Implications of thermomechanical modeling, *Geosphere*, *8*(6), 1286–1309, doi:10.1130/GES00746.1.

Saleeby, J., Z. Saleeby, and L. Le Pourhiet (2013), Epeirogenic transients related to mantle lithosphere removal in the southern Sierra Nevada region, California: Part II. Implications of rock uplift and basin subsidence relations, *Geosphere*, *9*(3), 394–425, doi:10.1130/GES00816.1.

Saltus, R. W., and A. H. Lachenbruch (1991), Thermal evolution of the Sierra Nevada: Tectonic implications of new heat flow data, *Tectonics*, *10*(2), 325–344, doi:10.1029/90TC02681.

Schutt, D. L., and C. E. Lesher (2010), Compositional trends among Kaapvaal Craton garnet peridotite xenoliths and their effects on seismic velocity and density, *Earth Planet. Sci. Lett.*, *300*(3–4), 367–373, doi:10.1016/j.epsl.2010.10.018.

Stern, T., G. Houseman, M. Salmon, and L. Evans (2013), Instability of a lithospheric step beneath western North Island, New Zealand, *Geology*, *41*(4), 423–426, doi:10.1130/G34028.1.

Thurber, C., H. Zhang, T. Brocher, and V. Langenheim (2009), Regional three-dimensional seismic velocity model of the crust and uppermost mantle of northern California, *J. Geophys. Res.*, *114*, B01304, doi:10.1029/2008JB005766.

Unruh, J., E. Hauksson, and C. H. Jones (2014), Internal deformation of the southern Sierra Nevada microplate associated with foundering lower lithosphere, California, *Geosphere*, *10*(1), 107–128, doi:10.1130/GES00936.1.

Wang, Y., D. W. Forsyth, C. J. Rau, N. Carriero, B. Schmandt, J. B. Gaherty, and B. Savage (2013), Fossil slabs attached to unsubducted fragments of the Farallon plate, *Proc. Natl. Acad. Sci. U.S.A.*, *110*(14), 5342–5346, doi:10.1073/pnas.1214880110.

Watts, A. B. (2001), *Isostasy and Flexure of the Lithosphere*, 458 pp., Cambridge Univ. Press, Cambridge.

Wentworth, C. M., G. R. Fisher, P. Levine, and R. C. Jachens (1995), revised 2007, The surface of crystalline basement, Great Valley and Sierra Nevada, California: A digital map database, *U.S. Geol. Surv. Open File Rep. 95-96*, vol. 1.1, 18 pp. [Available at http://pubs.usgs.gov/of/1995/96/.]

Yang, Y., and D. W. Forsyth (2006), Rayleigh wave phase velocities, small-scale convection, and azimuthal anisotropy beneath southern California, *J. Geophys. Res.*, *111*, B07306, doi:10.1029/2005JB004180.

Zandt, G. (2003), The southern Sierra Nevada drip and the mantle wind direction beneath the southwestern United States, *Int. Geol. Rev.*, *45*(3), 213–224, doi:10.2747/0020-6814.45.3.213.

Zandt, G., H. Gilbert, T. J. Owens, J. Saleeby, and C. H. Jones (2004), Active foundering of a continental arc root beneath the southern Sierra Nevada in California, *Nature*, *431*, 1–6.